IEEE Access
Multidisciplinary ⋮ Rapid Review ⋮ Open Access Journal

Received May 11, 2020, accepted June 18, 2020, date of publication June 22, 2020, date of current version July 2, 2020.

Digital Object Identifier 10.1109/ACCESS.2020.3004113

Model-Based Load Characteristics Analysis of the Multi-Dimensional Force Sensor

LIYUE FU, (Student Member, IEEE), AND AIGUO SONG, (Senior Member, IEEE)
State Key Laboratory of Bioelectronics, Southeast University, Nanjing 210096, China
Jiangsu Key Lab of Remote Measurement and Control, School of Instrument Science and Engineering, Southeast University, Nanjing 210096, China

Corresponding author: Aiguo Song (a.g.song@seu.edu.cn)

This work was supported in part by the National Key Research and Development Program of China under Grant 2016YFB1001301, in part by the National Natural Science Foundation of China under Grant U1713210, and in part by the National Key Research and Development Program of China under Grant 2017YFB1300305.

ABSTRACT As an important component of force feedback devices, the multi-dimensional force sensor (MDFS) has been widely used in haptic devices, prosthetic hands, and other devices. The structural distribution of the stiffness and mass of an MDFS is key to deeply understand its dynamic performance. To obtain this information, a model-based method for load characteristics analysis of the MDFS is proposed in this paper. The dynamic behavior of the force sensor for a given load is described by a lumped mass model consisting of spring-mass-damper elements and characterized by the model parameters that describe the dynamic correlation distribution of mass, stiffness, and damping. Compared with the results of finite element analysis (FEA) and the spectrum analysis of the step response, the natural frequencies with different load masses are in accordance with the model based on the proposed method. The main purpose of the proposed method is the description of the load characteristics of the MDFS, independent of the given mechanical environment, which provides a certain theoretical reference for the calculation of the load capacity of the force sensor. Meanwhile, in order to improve the dynamic performance, a dynamic compensated filter is added to the force sensor coupling system, thereby broadening the operation frequency and greatly reducing the response time.

INDEX TERMS Differential evolution, load characteristics, lumped mass model, multi-dimensional force sensor.

I. INTRODUCTION

The past two decades have shown remarkable advances in the field of virtual reality (VR). It is important to provide good haptic feedback in order to obtain information about contact with the objects in the virtual environment [1]. Most researches have primarily focused on studies of fast and accurate collision detection algorithm [2] and simulating haptic properties of objects [3]. As the interface equipment of the human-computer interaction, force feedback device provides the operators with the information of weight, hardness, inertia and so on close to the real environment, which enhances the operator's sense of reality and immersion. The multi-dimensional force sensor (MDFS), regarded as an important component of force feedback devices, has been widely applied in virtual reality, teleoperation robots, rehabilitation robots, minimally invasive surgery, biomechanical applications, and so on [4]–[8]. The force feedback device senses force feedback information in real time based on the MDFS and adjusts a system's operation, thus realizing fast, accurate, and efficient haptic interaction. Nevertheless, in order to achieve this goal, the MDFS must have good dynamic performance [9], including good load characteristics [10]. Multi-dimensional dynamic forces play a critical role as the basic information of the control process. However, the dynamic operation of the force sensor in the loaded state under the guidance of the dynamic characteristics of the force sensor in the unloaded state may lead to inaccuracies and instabilities, and the dynamic performances of the force sensor with different loads are distinct. Furthermore, in heavy-load operations, the frequency response characteristics of many force feedback devices are poor [11]. Increasing demands for higher accuracy dynamic force measurement have highlighted the fact that there is a lack of analysis of the

The associate editor coordinating the review of this manuscript and approving it for publication was Md. Moinul Hossain.

dynamic characteristics of force sensors, especially the load characteristics of MDFS [12].

In recent years, great progress has been made in static decoupling of MDFS. However, studies on the dynamic characteristics of MDFS are few. Song *et al.* [13] presented a novel self-decoupled four-dimensional force/torque sensor, which is a direct output force sensor. Ma *et al.* [14] proposed a decoupling algorithm for three-dimensional force sensors based on a coupling error model and ε–SVR, and this algorithm gave more robust performance with high efficiency and decoupling accuracy. Park *et al.* [15] evaluated the dynamic characteristics of a binocular force/torque sensor by using a shaker system, but the calibration quality and frequency range were limited due to the shaker system used. In [12], the transfer characteristics of a 6-axis force measuring system were seen as a second-order linear time-invariant system. An impulse response experiment [16] was conducted to dynamically calibrate the force sensor, and the test results indicated that the bandwidth of the piezoelectric 6-axis force sensor was near 2000 Hz. Wang *et al.* [17] analyzed the dynamic force response of a parallel pre-stressed six-axis force sensor but could only obtain the analytical expressions between the dynamic response of the sensor and the differential equations of motion. Liu *et al.* [18] established an analytical mathematical model and a numerical simulation model of a planar piezoelectric six-axis force/torque sensor and analyzed the amplitude-frequency characteristics using the harmonic response
method.

A key step of analysis of dynamic characteristics of measurement system is dynamic modeling. Particularly, a great deal of dynamic modeling approaches for compliant mechanisms have been reported in a growing stream of publication [19]. For example, a Pseudo-Rigid-Body Model based dynamic model for parallel-guided compliant mechanism [20] was presented by Yu *et al.* Rösner *et al.* [21] developed a novel approach towards dynamical modeling of compliant mechanisms mostly flexure hinges, which provides efficient approximations for model order reduction procedures. Afterwards, Ling *et al.* proposed a semi-analytical finite element model [22]. However, this approach requires cumbersome inner-force and kinematic analyses, and the prediction accuracy for high-order frequency is limited. To address these problems, a dynamic stiffness matrix based pseudo-static modeling method [23] for compliant mechanisms were developed by Ling *et al.* This method can model the simultaneous kinetostatics and dynamics of compliant mechanisms with small deflection in a static manner. At present, it has been widely used in a variety of high-dynamic applications.

Bandwidth is the most practical dynamic performance index of the sensor and test system [24], and the natural frequency is related not only to the structure of the system but also to the load it carries. For example, when a manipulator grabs objects of different masses, the dynamic performance of the whole test system with the MDFS will change. Generally speaking, with the increase of the load mass, the bandwidth will get lower [25]. Nevertheless, the quantitative relationship between the bandwidth and the load mass needs to be further studied.

The resonance of a mechanical structure depends on its elastically coupled mass elements. Low stiffness and light damping lead to increased forced vibrations and process instability [11], [15]. In a given application, both ends of the force sensor are always coupled with the mechanical environment by a screw thread, which may result in a totally different dynamic behavior from a bare force sensor [26], [27]. Fundamental resonance is not enough to understand the dynamic behavior of a force sensor in a specific application. Instead, it is important to have information about the structural distribution of the sensor's stiffness and mass, which are the key pieces of data for understanding the sensor's dynamic performance in depth [28].

To address this need, this paper presents a model-based method to analyze the dynamic performance, including the load characteristics, of the MDFS. In this method, the dynamic behavior of the MDFS in a given mechanical environment is described by a lumped mass model consisting of a spring, mass, and damper elements and characterized by the model parameters that describe the dynamic correlation distribution of mass, stiffness, and damping. The main purpose of the proposed approach is the description of the dynamic behavior of the MDFS, especially its load characteristics, independent of the given mechanical environment.

The performance requirements of the MDFS are different in different applications. In the biomechanical measurement system of astronauts, the requirements of the dynamic performance of the MDFS are low as a result of the low movement frequency of astronauts. In micromachining and high-speed machining, dynamic cutting force measurement is performed by using multi-axis force sensors [29], [30]. Since the frequency of the micromachining force is high to thousands of hertz due to the use of high-speed spindles [31], the effective bandwidth of the multi-axis force sensor needs to be extended. Hence, the dynamic compensation filter is used to compensate the dynamic performance of the MDFS in this paper.

The organization of this paper is as follows: Section 2 introduces the dynamic calibration devices and the dynamic tests conducted to experimentally analyze the load characteristics of the MDFS. Section 3 describes the finite element analysis (FEA) of the MDFS and coupling system with different load masses. In Section 4, the setup of a lumped mass model of the system is explained, and the model parameters are identified from the step response of the system in dynamic force measurements. For the sake of improving the dynamic performance of the system, a dynamic compensated filter is added to the system as discussed in Section 5. Section 6 details a verification test by a human-machine interaction force feedback device. In Section 7, the conclusions of the study are presented.

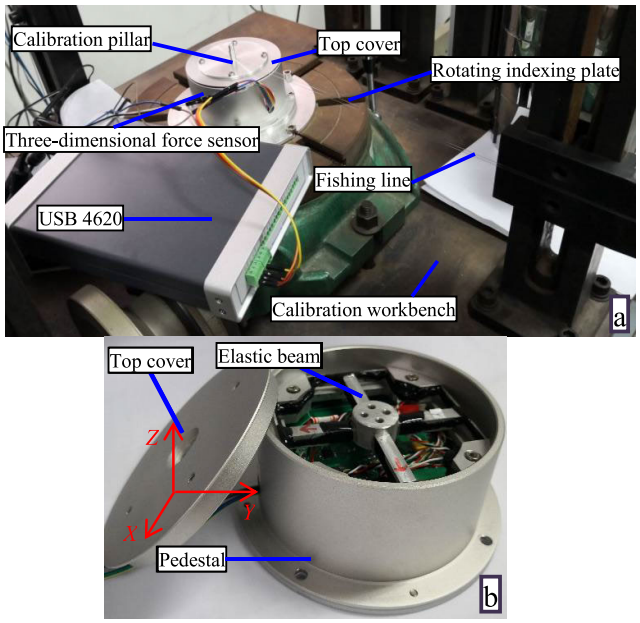

FIGURE 1. Dynamic calibration device and three-dimensional force sensor.

FIGURE 2. (a) Four mass bodies used in dynamic calibration test: 8 g, 48 g, 98 g, and 198 g. (b) Load mass 8 g. (c) Load mass 198 g.

II. EXPERIMENTAL TESTS

A. DYNAMIC CALIBRATION DEVICE

Fig. 1(a) illustrates the dynamic calibration device of the MDFS. The MDFS developed by Southeast University is a resistance strain type sensor, as shown in Fig. 1(b). A step response method is used to dynamically calibrate the MDFS, which is installed on the test bench along a certain direction. The excitation force applied to the sensor through the calibration pillar causes deformation of the elastic element. One end of the rope (fishing line) is hung on the calibration pillar of the MDFS, and the other end suspends the weight by a pulley. The stretching direction of the rope must be in a straight line with the dimension of the MDFS to be tested. The rope is cut off at a given time, thus applying a negative step excitation to the calibration pillar, which transfers the excitation to the MDFS's elastic beam [32]. The excitation leads to the elastic beam's vibration deformation and the change of the output voltage of the MDFS's test channel. It is noted that, in the case of dynamic events, it is necessary to ensure a sufficiently high cut-off frequency for the low-pass amplifier in the filter settings (recommendation: approx. 20% higher than the signal frequency) [33]. If the influences of the circuit board mass and the cutoff frequency of the amplifier are ignored, the frequency characteristics of the output voltage of the force sensor reflect the frequency characteristics of the whole test system, including the MDFS.

Higher mounting torque will result in harder thread connection; accordingly, it could lead to higher resonance frequencies. Therefore, we should install and assemble the sensor with higher mounting torque in a safe range while using the sensor.

Five different load cases are selected to test the load characteristics of the force sensor coupling system, which are without a load and with a load mass of 8, 48, 98, and 198 g. Fig. 2 displays the four mass bodies used in the experiment as well as the experimental setups of two load cases.

B. DYNAMIC FORCE MEASUREMENT

Fig. 3 shows the step responses of the force sensor with different loads. Due to the very small damping of the system, the oscillation is violent, and the overshoot is very large. In addition to a signal of a certain frequency generated by the characteristics of the system itself, as the load mass increases, a signal of another frequency is enhanced. The specific value of the frequency needs to be acquired by further spectrum analysis.

As depicted in Fig. 4, the amplitude-frequency responses of output signals are obtained by discrete Fourier transform (DFT), and such a modification of the load mass mounted on the sensor alters the dynamic response of the MDFS. Two load-related resonances are shown in the spectrum. The first-order resonances are generated by the elastic coupling between the elastic beam and the base of the sensor, and second-order resonances are generated by the elastic coupling between the beam and the load mounted on the sensor. The first-order resonance frequencies of the five load cases are 500, 486, 450, 393, and 320 Hz. When the load mass is small, the stiffness between the load and the elastic beam of the force sensor is high enough that the second-order resonance of low energy can be neglected. With the increase of load mass, the connection becomes an elastic coupling, which makes the second-order resonance move to the low frequency region, and its amplitude noticeably increases.

III. FINITE ELEMENT ANALYSIS

It is necessary to perform the Modal Analysis and Harmonic Analysis via FEA software in order to detect the resonance response and the maximum safe frequency range of the force

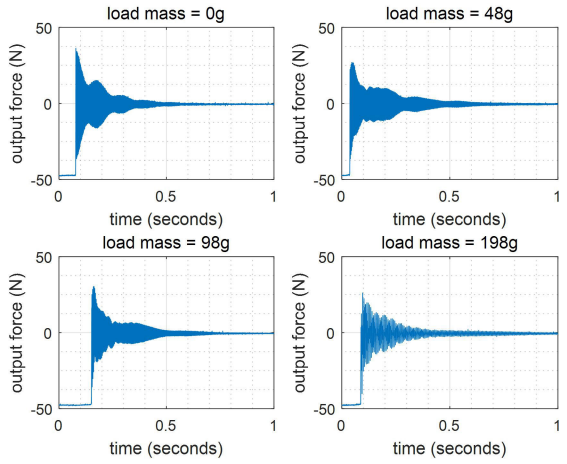

FIGURE 3. Step response of the three-dimensional force sensor measured under different loads.

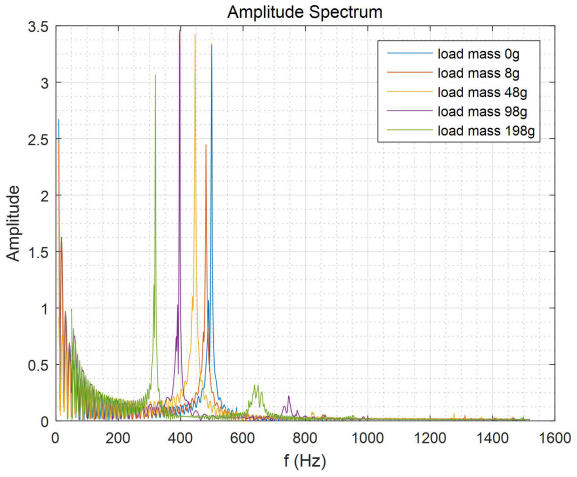

FIGURE 4. Amplitude spectrum of the step response for the three-dimensional force sensor obtained with different loads measured at the dynamic calibration test bench.

sensor coupling system. Since the pedestal of the force sensor is fixed on the rotating indexing plate of the calibration workbench, it can be considered that the connection between the pedestal and the workbench is rigid. Consequently, in the FEA of the sensor coupling system, the influence of the pedestal can be ignored, that is, the system composed of elastic beam, top cover, calibration pillar, and load mass, as illustrated in Fig. 5, is analyzed.

The FEA of the force sensor coupling system under different load masses is carried out, and the first-order vibration mode and frequency responses of the system are obtained, as depicted in Figs. 6 and 7, respectively.

IV. MODELING AND PARAMETERS IDENTIFICATION

A. ANALYTICALLY DYNAMIC MODEL

For the model of the force sensor coupling system, the elastic couplings at both ends of the MDFS should be considered in order to obtain a sound understanding of the dynamic

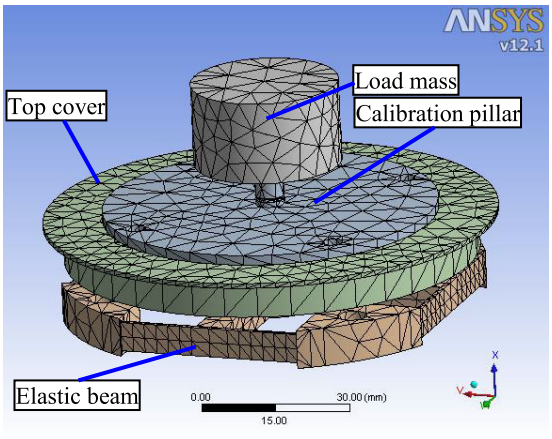

FIGURE 5. Finite element model of the force sensor coupling system.

behavior independent of the experimental setup. For the sake of description of the dynamic behavior, the MDFS and its dynamic calibration system are modeled by a spring-mass-damper system (Fig. 8), which consists of three lumped masses (m_B, m_E, m_L) with a linear elastic element between two of them. Here, m_B, m_E, and m_L represent the masses of the base, elastic beam, and load of the MDFS, respectively; k, c denote the equivalent stiffness and damping between the base and the elastic beam, respectively; k_L, c_L are the equivalent stiffness and damping between the elastic beam and the load, respectively. The mass body motions are described by the linear displacement coordinates (x_B, x_E, and x_L). The force f_S represents the dynamic force applied to the MDFS during dynamic calibration. The model's output is the output voltage U_F of the MDFS proportional to the expansion of the elastic element and is given by

$$U_F = n \cdot x_E, \tag{1}$$

where n denotes a scaling factor.

The dynamic behavior of the model can be described by a linear ordinary differential equation (ODE), which is deduced from the force balance conditions of the lumped masses. The ODE is as follows:

$$\begin{cases} m_L\ddot{x}_L + c_L\left(\dot{x}_L - \dot{x}_E\right) + k_L\left(x_L - x_E\right) = f_S \\ m_E\ddot{x}_E - c_L\left(\dot{x}_L - \dot{x}_E\right) + c\dot{x}_E - k_L\left(x_L - x_E\right) + kx_E = 0. \end{cases} \tag{2}$$

where, x_E and x_E represent the displacements of the elastic beam and the load, respectively; $\dot{x}_E$ and $\dot{x}_L$ denote the velocities of the elastic beam and the load, respectively; $\ddot{x}_E$ and $\ddot{x}_L$ denote the accelerations of the elastic beam and the load, respectively.

It is assumed that x_S and F_S are the Laplace transforms of the displacement vector x and the exerted force F, respectively. Thus, the transfer function of the system can be solved by Laplace transform as follows:

$$H(s) = \frac{L\left[U_F\right]}{L\left[f_S\right]} = \frac{n \cdot X_E(s)}{F(s)} = \frac{A(s)}{B(s)}, \tag{3}$$

$$A(s) = n\left(sc_L + k_L\right), \tag{3a}$$

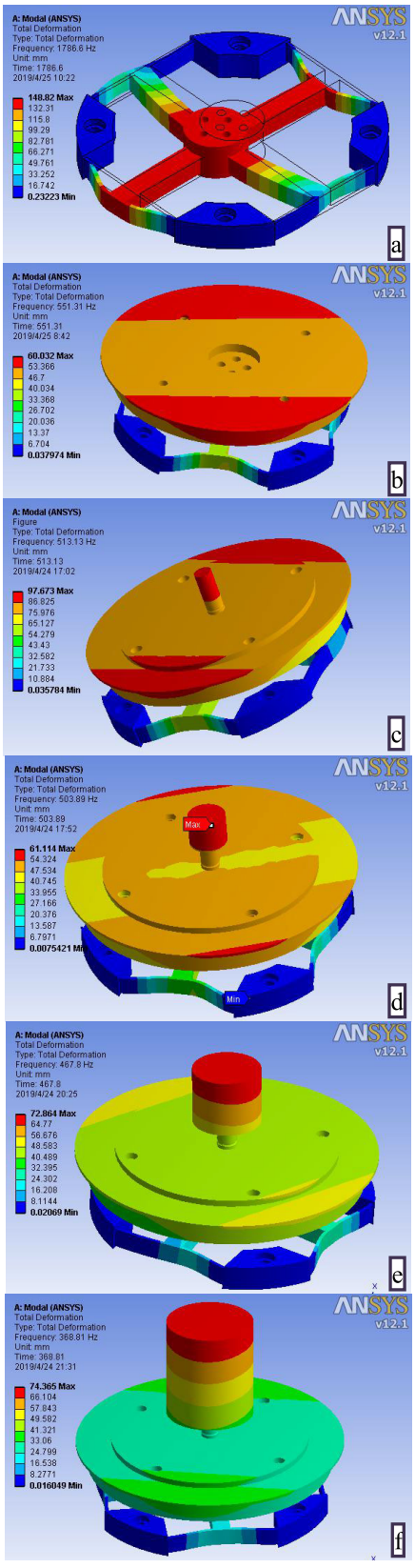

FIGURE 6. First-order vibration mode of the force sensor coupling system under different cases: (a) elastic beam; (b) elastic beam and top cover; (c) load mass = 0 g; (d) load mass = 8 g; (e) load mass = 48 g; and (f) load mass = 198 g.

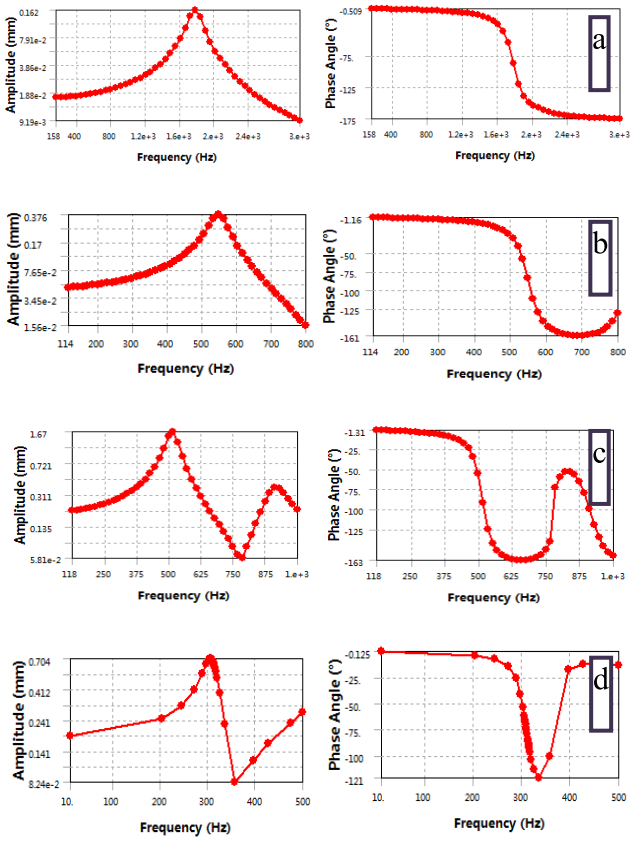

FIGURE 7. Frequency response of the force sensor coupling system under different cases: (a) elastic beam; (b) elastic beam and top cover; (c) load mass = 0 g; and (d) load mass = 198 g.

$$B(s) = s^4 m_L m_E + s^3 \left[m_L (c + c_L) + m_E c_L\right] + s^2 \left[m_L (k + k_L) + c c_L + m_E k_L\right] + s (k c_L + c k_L) + k k_L \tag{3b}$$

The coupling between m_E and m_L can be considered as a rigid coupling when the load mass m_L is very small. Hence, the three-mass model of the system can be simplified to a two-mass model, as depicted in Fig. 9. Equation (4) illustrates the ODE in order to describe the dynamic behavior of the model:

$$(m_E + m_L)\,\ddot{x}_\varepsilon + c\dot{x}_E + k x_E = f_S. \tag{4}$$

The transfer function of the MDFS and its coupling system can be expressed as follows:

$$H(s) = n/\left[(m_E + m_L)\,s^2 + cs + k\right]. \tag{5}$$

For the neglected damping model, the resonance frequency can be written as

$$\omega = \sqrt{k/(m_E + m_L)}. \tag{6}$$

It can be seen from the aforementioned equations that the frequency characteristics are related to the load mass

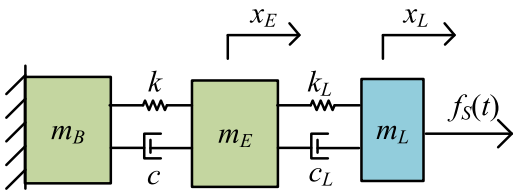

FIGURE 8. Three-mass model of the MDFS coupling system.

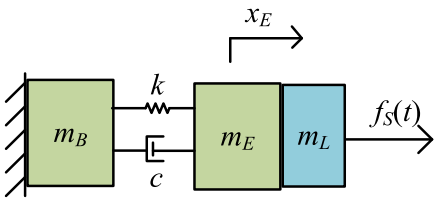

FIGURE 9. Two-mass model of the MDFS coupling system.

(i.e., the load characteristics). When the load is small, the natural frequency of the MDFS coupling system is inversely proportional to the square root of the load mass. Consequently, we only need to find a way to figure out the parameters (k, c, k_Lk$_L$, c_Lc$_L$) of the model shown in Fig. 8 or 9, and then we can get the characteristics of any required load.

It must be noted that each direction of the MDFS coupling system needs to be modeled, and different models have different equivalent stiffness and damping. However, this only applies to the case without consideration of dynamic (frequency-dependent) cross-talk. A comprehensive dynamic model for all the three directions needs to be built taking into account dynamic cross-talk, and then perform dynamic decoupling. The cross-talk of the three-dimensional force sensor is small, so the effect of cross-talk is ignored.

B. MODEL PARAMETERS IDENTIFICATION

The measured data acquired from the dynamic calibration experiment are the output voltages of one dimension of the force sensor. When the connection between the load and the force sensor is rigid, the system can be simplified to a two-mass model and the second-order resonance can be neglected. The transfer function of the coupling system can be expressed by Equation (5).

If the system is approximately regarded as a second-order system, the time-domain performance indices can be obtained from the transient process curve of the MDFS coupling system. First, we can get the oscillating period T of the step response, and then we can get the oscillating frequency as Equation (7). Moreover, the overshoot can be obtained, as shown in Equation (8), by the peak and steady-state values of the response. It can be seen that the overshoot is very large:

$$\omega_d = 3140\text{rad/s}. \tag{7}$$

$$\sigma\% = 92.6\%. \tag{8}$$

The damping ratio is an important parameter of a control system. In terms of the relationship between the overshoot and the damping ratio of the second-order system (as expressed by Equation (9)), the damping ratio of the

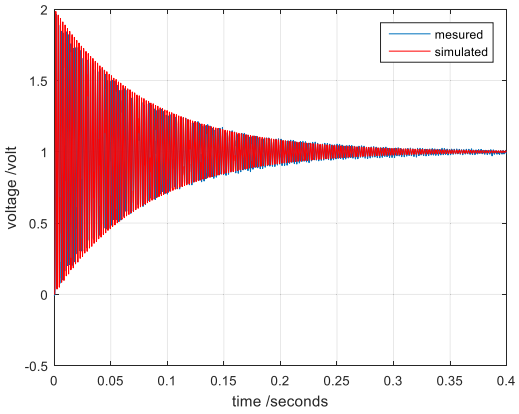

FIGURE 10. Comparison chart of step responses of experimental measurement and model simulation.

TABLE 1. The masses of components of the sensor coupling system.

components	Mass (grams)
Pedestal (base) m_b	161
Elastic beam m_E	89
Top cover m_t	130
Calibration pillar m_p	21
Load m_L	8
	48
	98
	198

MDFS coupling system can be calculated as Equation (10). The damping ratio of the system is very low, so it is urgent to implement dynamic compensation for the system, which is introduced in the next section.

$$\sigma\% = e^{-\zeta\pi}\sqrt{1-\zeta^2}. \tag{9}$$

$$\zeta = 0.004. \tag{10}$$

For the very low damping ratio, the natural frequency is approximately equal to the oscillating frequency of the system, (i.e., $\omega_n = \omega_d = 3140 rad/s$), which is consistent with the frequency spectrum of the step response and also in accordance with the FEA result. Furthermore, the transfer function of the system can be written as

$$G(s) = \frac{9.86 \times 10^6}{s^2 + 25s + 9.86 \times 10^6} \tag{11}$$

The step response of the model is compared with the measured step response, as shown in Fig. 10. It can be seen that the two responses fit well, and the model can be used.

Combining Equations (5) and (11), we can get the following equations:

$$\begin{cases} c/(m_E + m_L) = 25 \\ k/(m_E + m_L) = 9.86 \times 10^6. \end{cases} \tag{12}$$

The masses of each component of the sensor coupling system are listed in Table 1. Therefore,

$$\begin{cases} c = 6 \\ k = 2.36 \times 10^6. \end{cases} \tag{13}$$

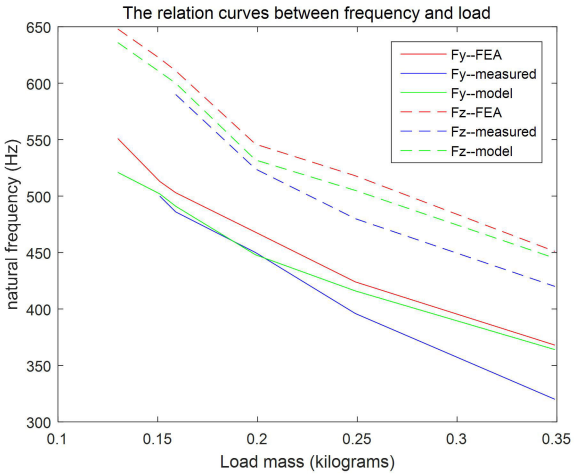

FIGURE 11. The relationship between natural frequency and load mass.

TABLE 2. Natural frequencies of the sensor coupling system with different loads.

Cases	*Fy*				*Fz*			
	f_1 (Hz)	f_2 (Hz)	f_3 (Hz)	d (%)	f_1 (Hz)	f_2 (Hz)	f_3 (Hz)	d (%)
Only m_t	551	/	521	/	648	/	636	/
Load: 0	513	500	502	0.4	622	/	610	/
Load: 8 g	503	486	491	1	611	590	600	1.7
Load: 48 g	468	450	448	0.45	546	524	532	1.5
Load: 98 g	424	393	414	5.1	518	480	505	4.9
Load:198 g	368	320	364	12	451	420	445	5.6

Accordingly, we can get the relationship between the natural frequency and the load mass of the coupling system as follows:

$$\omega_n = \sqrt{\frac{2.36 \times 10^6}{0.089 + m_L}}, \tag{14}$$

where m_L includes not only the mass of the load body as illustrated in Fig. 2(a) but also the masses of the top cover (m_t) and the calibration pillar (m_p).

It must be noted that all the above analyses are in Fy dimension of the MDFS. Analyses in other dimensions are performed in the same way. Fig. 11 and Table 2 visualize the relationship between the natural frequency and the load mass under three cases. Here, f_1, f_2, and f_3 denote the natural frequencies obtained from FEA, the experiment, and the model, respectively; d represents the mathematical model's relative error compared to the experimental result. Because of the symmetry of the elastic beam, the performances of the MDFS in X and Y directions are essentially the same.

It can be seen in Fig. 11 that the natural frequency of the system measured in the experiment is smaller than that obtained by FEA, and the calculated value of the model is between these two results but closer to the results of FEA. The reason for this phenomenon is that the basic idea of FEA is to constrain an infinite dimension problem as a finite dimension problem. Consequently, according to the Rayleigh constraint theorem, the frequency of FEA, which is the upper bound of the frequency value, is higher than the measured value. Based on the assumption of the bonded connection between the components during FEA, the resulting natural frequency is the highest of all possible cases. It can also be seen that, with the increase of the load mass, the difference between the measured value and the model's calculated value increases; and the relative error is more than 5% when the load mass is increased to 98 g. Therefore, if 5% is defined as the allowable limits of error (ALE), the final equivalent stiffness (as shown in Eq. (13)) calculated from the two-mass model is only suitable to the load whose mass is less than 98 g.

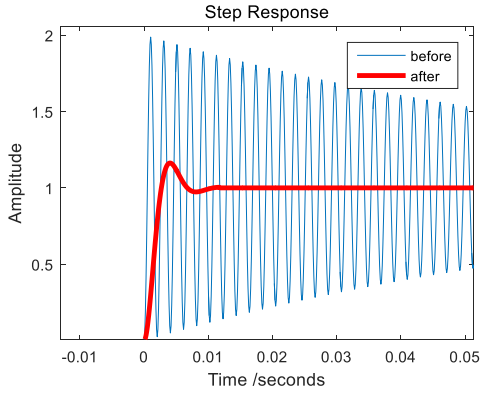

FIGURE 12. The step response of the system before and after compensation.

V. DYNAMIC PERFORMANCE COMPENSATION

Apparently, the oscillation of the step response of the MDFS coupling system is very intense, and the response time is very long. Thus, the dynamic performance is very poor, and it is urgent to add a dynamic compensated filter to the system. If we hope to increase the natural frequency and the damping ratio to 1000 Hz and 0.5, respectively, the transfer function of the system after compensation is

$$H(s) = G_0(s) \cdot G_c(s) = \frac{3.94 \times 10^7}{s^2 + 6280s + 3.94 \times 10^7}, \tag{15}$$

where $G_0(s)$ and $G_c(s)$ are the transfer functions of the original system and the compensated filter, respectively, and they are expressed as follows:

$$G_0\,(\mathrm{s}) = \frac{2.36 \times 10^6}{(0.089 + m_L)\, s^2 + 6s + 2.36 \times 10^6} \tag{16}$$

$$G_c\,(\mathrm{s}) = \frac{[(0.089 + m_L)\, s^2 + 6s + 2.36 \times 10^6] \times 16.7}{s^2 + 6280s + 3.94 \times 10^7} \tag{17}$$

The step responses and Bode plots of the MDFS coupling system without load (just calibration pillar, i.e. $m_L = 0.151$kg in Eq. (16)) before and after compensation are depicted in Fig. 12 and 13, respectively. It can be seen that the response time is greatly reduced, and the bandwidth with an amplitude

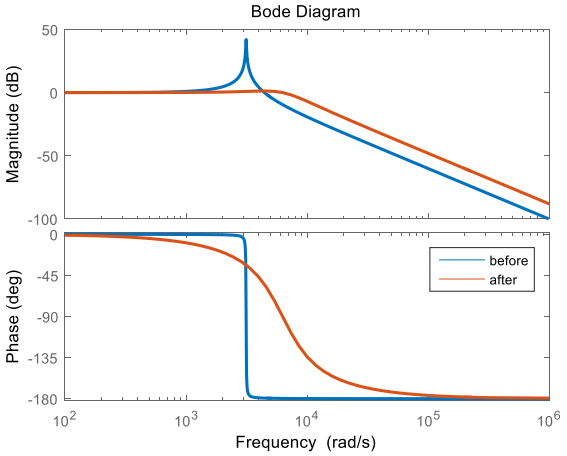

FIGURE 13. Bode plots of the MDFS coupling system before and after dynamic compensation.

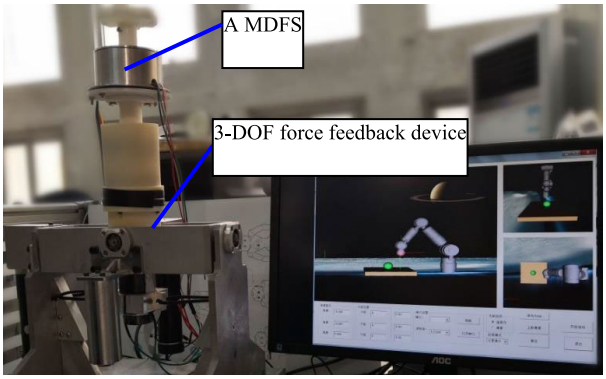

FIGURE 14. Force feedback test conducted by a haptic device including a three-dimensional force sensor.

error of ±10% broadened from 490 Hz to 1,560 Hz, which means the dynamic performance of the MDFS coupling system is greatly improved with the addition of the dynamic compensated filter.

VI. VERIFICATION TEST

As shown in Fig. 14, a three-degrees-of-freedom (3-DOF) human-machine interaction force feedback device is used to control the movement of a manipulator in a virtual environment to grab a ball for a force feedback test. The feedback forces F_v in all directions and the user-applied forces F_u to the haptic device are recorded during the test. In the experiment, the rigid spring model is used to calculate the feedback force, that is, when the force feedback virtual particle in the virtual environment collides with the target colliding object, the feedback force begins to be generated. The smaller the distance between the particle and the center point of the target, the greater the feedback force.

The user-applied forces F_u to the haptic device (the steering handle) sensed from the MDFS are compared with the feedback forces F_v from the virtual environment. Fig. 15(a) and (b) display the contrast diagrams when the load characteristics of the MDFS are not considered and are considered, respectively. It can be seen from the figure that the dynamic

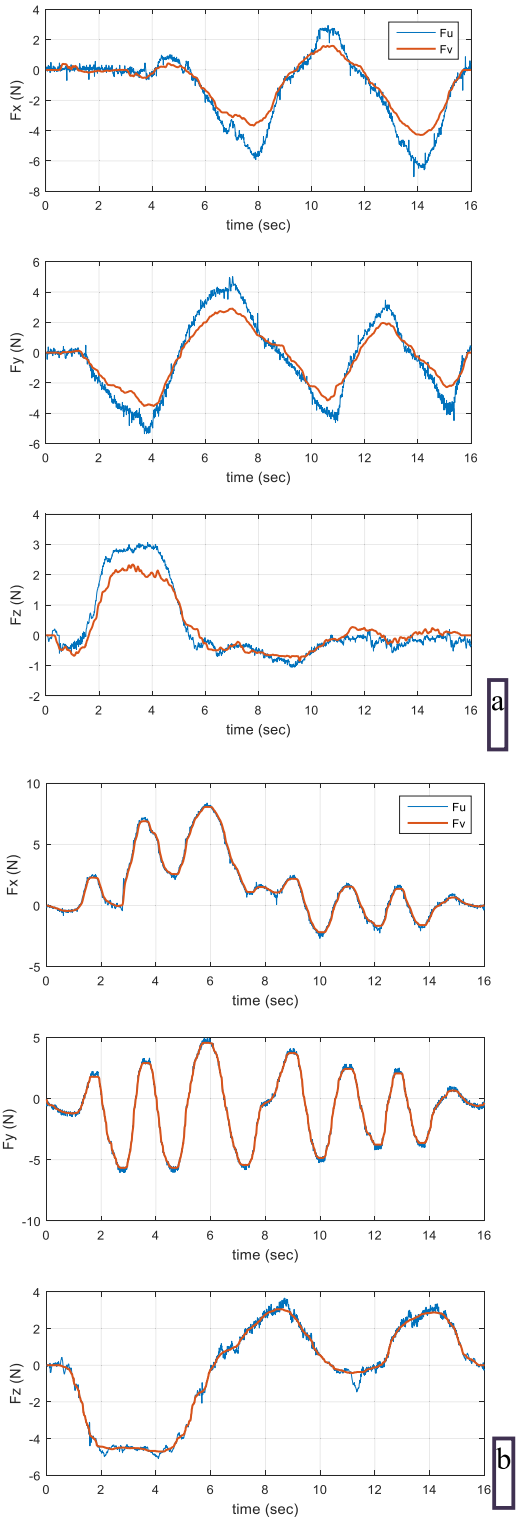

FIGURE 15. Comparison between the user-applied force and the feedback force of the haptic device (a) without consideration of load characteristics and (b) with consideration of load characteristics.

forces caused by manipulating the steering handle are well tracked and compensated after considering the load characteristics of the three-dimensional force sensor.

VII. CONCLUSION AND DISCUSSION

An approach for the model-based load characteristics analysis of the MDFS is proposed in this paper. The qualitative relationship between the natural frequency and load mass is obtained by spectrum analysis of the step response of the MDFS in different load cases. The quantitative relationship is obtained by a lumped mass model consisting of a spring, mass, and damper, which describes the dynamic behavior of the force sensor in a given mechanical environment. When the load is small, the natural frequency of the MDFS is inversely proportional to the square root of the load mass.

The motion of the internal masses of the force sensor is mainly affected by inertia and elasticity. Elasticity is primarily generated by the material of the elastic beam of the force sensor and the coupling between the sensor and mechanical environment. Inertia force generated by the mass component of the elastic coupling structure during dynamic testing has an impact on dynamic measurement behavior. That is one of the main reasons why the natural frequency varies with the load mass.

Although the proposed model-based method can achieve the analysis of the load characteristics of the MDFS, there are still some shortcomings in this paper. For example, we also need to consider the frequency responses of the signal conditioning and amplifier to guarantee their reasonable bandwidths. When the size of the load exceeds a certain threshold, the elastic coupling between the elastic beam and the load must be considered, and the system must be regarded as a high-order system. Thus, we need to find a suitable model identification method to accurately identify the parameters of the lumped mass model.

ACKNOWLEDGMENT

The authors thank LetPub (www.letpub.com) for its linguistic assistance during the preparation of this manuscript. This article was presented in part at the International Conference on Control, Automation and Systems (ICCAS 2019).

REFERENCES

[1] F. P. Brooks, "What's real about virtual reality," *IEEE Comput. Graph. Appl.*, vol. 19, no. 6, pp. 16–27, Nov./Dec. 1999.

[2] A. Gregory, M. C. Lin, S. Gottschalk, and R. Taylor, "Fast and accurate collision detection for haptic interaction using a three degree-of-freedom force-feedback device," *Comput. Geometry*, vol. 15, nos. 1–3, pp. 69–89, Feb. 2000.

[3] S. Das, C. Thakur, and Y. Kurita, "Force-feedback in virtual reality through PGM-based ForceHand glove," in *Proc. IEEE/SICE Int. Symp. Syst. Integr. (SII)*, Jan. 2020, pp. 1016–1021.

[4] E. Korkmaz, B. A. Gozen, B. Bediz, and O. B. Ozdoganlar, "High-frequency compensation of dynamic distortions in micromachining force measurements," *Procedia Manuf.*, vol. 1, pp. 534–545, Jan. 2015.

[5] B.-L. Wu, D.-K. Qu, and F. Xu, "Industrial robot high precision peg-in-hole assembly based on hybrid force/position control," *J. Zhejiang Univ. (Eng. Sci.)*, vol. 52, no. 2, pp. 379–386, 2018.

[6] E. Kyrkjebø, "Inertial human motion estimation for physical human-robot interaction using an interaction velocity update to reduce drift," in *Proc. Companion ACM/IEEE Int. Conf. Hum.-Robot Interact.*, Mar. 2018, pp. 163–164.

[7] D.-H. Lee, U. Kim, H. Jung, and H. R. Choi, "A capacitive-type novel six-axis Force/Torque sensor for robotic applications," *IEEE Sensors J.*, vol. 16, no. 8, pp. 2290–2299, Apr. 2016.

[8] R. A. Brookhuis, H. Droogendijk, M. J. de Boer, R. G. P. Sanders, T. S. J. Lammerink, R. J. Wiegerink, and G. J. M. Krijnen, "Six-axis force-torque sensor with a large range for biomechanical applications," *J. Micromech. Microeng.*, vol. 24, no. 3, pp. 5015–5024, 2014.

[9] Y.-Q. Leng, Z.-C. Chen, X. He, Y. Zhang, and W. Zhang, "Collision sensing using force/torque sensor," *J. Sensors*, vol. 2016, Jan. 2016, Art. no. 6291216.

[10] K. Li, B. Pan, Y. Fu, and S. Wang, "Experimental study of static and dynamic characteristics of a miniature 6-axis force and torque sensor," in *Proc. IEEE Int. Conf. Inf. Autom.*, Aug. 2015, pp. 1579–1584.

[11] Y.-J. Li, G.-C. Wang, J. Zhang, and Z.-Y. Jia, "Dynamic characteristics of piezoelectric six-dimensional heavy force/moment sensor for large-load robotic manipulator," *Measurement*, vol. 45, no. 5, pp. 1114–1125, Jun. 2012.

[12] D. Prattichizzo, F. Chinello, C. Pacchierotti, and M. Malvezzi, "Towards wearability in fingertip haptics: A 3-DoF wearable device for cutaneous force feedback," *IEEE Trans. Haptics*, vol. 6, no. 4, pp. 506–516, Oct. 2013.

[13] A. Song, J. Wu, G. Qin, and W. Huang, "A novel self-decoupled four degree-of-freedom wrist force/torque sensor," *Measurement*, vol. 40, nos. 9–10, pp. 883–891, Nov. 2007.

[14] J. Ma and A. Song, "Fast estimation of strains for cross-beams six-axis force/torque sensors by mechanical modeling," *Sensors*, vol. 13, no. 5, pp. 6669–6686, May 2013.

[15] Y.-K. Park, R. Kumme, and D.-I. Kang, "Dynamic investigation of a binocular six-component force-moment sensor," *Meas. Sci. Technol.*, vol. 13, no. 8, pp. 1311–1318, Aug. 2002.

[16] M. H. Korayem, N. Ebrahimi, and M. S. Sotoudegan, "Frequency response of atomic force microscopy microcantilevers oscillating in a viscous liquid: A comparison of various methods," *Scientia Iranica*, vol. 18, no. 5, pp. 1116–1125, Oct. 2011.

[17] Z. Wang, J. Yao, H. Wang, Y. Hou, and Y. Zhao, "Dynamic force response analysis on parallel pre-stressed six-axis force sensor," *Robot*, vol. 33, no. 4, pp. 455–460, Sep. 2011.

[18] J. Liu, L. Zhang, Z. Fu, M. Li, J. Liu, and L. Qin, "Dynamic characteristic analysis of planar piezoelectric six-axis Force/Torque sensor," in *Proc. 10th Int. Conf. Intell. Hum.-Mach. Syst. Cybern. (IHMSC)*, Aug. 2018, pp. 140–145.

[19] M. Ling, L. L. Howell, J. Cao, and G. Chen, "Kinetostatic and dynamic modeling of flexure-based compliant mechanisms: A survey," *Appl. Mech. Rev.*, vol. 72, no. 3, May 2020.

[20] Y.-Q. Yu, L. L. Howell, C. Lusk, Y. Yue, and M.-G. He, "Dynamic modeling of compliant mechanisms based on the pseudo-rigid-body model," *J. Mech. Des.*, vol. 127, no. 4, pp. 760–765, Jul. 2005.

[21] M. Rösner, R. Lammering, and R. Friedrich, "Dynamic modeling and model order reduction of compliant mechanisms," *Precis. Eng.*, vol. 42, pp. 85–92, Oct. 2015.

[22] M. Ling, J. Cao, Z. Jiang, and J. Lin, "A semi-analytical modeling method for the static and dynamic analysis of complex compliant mechanism," *Precis. Eng.*, vol. 52, pp. 64–72, Apr. 2018.

[23] M. Ling, L. L. Howell, J. Cao, and Z. Jiang, "A pseudo-static model for dynamic analysis on frequency domain of distributed compliant mechanisms," *J. Mech. Robot.*, vol. 10, no. 5, Oct. 2018, Art. no. 051011.

[24] J. Huang, "Applied modeling method," in *Measurement System Dynamics and Application*, 1st ed. Beijing, China: National Defense Industry Press, 2013, pp. 51–88.

[25] M. Kobusch and S. Eichstädt, "A case study in model-based dynamic calibration of small strain gauge force transducers," *Acta Imeko*, vol. 6, no. 1, pp. 3–12, Apr. 2017.

[26] M. Kobusch, "Characterization of force transducers for dynamic measurements," *PTB-Mitteilungen*, vol. 125, no. 2, pp. 43–51, 2015.

[27] M. Kobusch, S. Eichstädt, L. Klaus, and T. Bruns, "Investigations for the model-based dynamic calibration of force transducers by using shock excitation," *Acta Imeko*, vol. 4, no. 2, pp. 45–51, Jun. 2015.

[28] M. H. Vu and U. J. Na, "A new 6-DOF haptic device for teleoperation of 6-DOF serial robots," *IEEE Trans. Instrum. Meas.*, vol. 60, no. 11, pp. 3510–3523, Nov. 2011.

[29] G. Totis and M. Sortino, "Development of a modular dynamometer for triaxial cutting force measurement in turning," *Int. J. Mach. Tools Manuf.*, vol. 51, no. 1, pp. 34–42, Jan. 2011.

[30] I. Kang, J. Kim, C. Hong, and J. Kim, "Development and evaluation of tool dynamometer for measuring high frequency cutting forces in micro milling," *Int. J. Precis. Eng. Manuf.*, vol. 11, no. 6, pp. 21–817, 2010.

[31] E. Korkmaz, B. A. Gozen, B. Bediz, and O. B. Ozdoganlar, "Accurate measurement of micromachining forces through dynamic compensation of dynamometers," *Precis. Eng.*, vol. 49, pp. 365–376, Jul. 2017.
[32] L. Fu and A. Song, "Dynamic characteristics analysis of the six-axis force/torque sensor," *J. Sensors*, vol. 2018, Jan. 2018, Art. no. 6216979, doi: 10.1155/2018/6216979.
[33] *DKD-R 3-10: Dynamic Calibration of Uniaxial Force Measuring Devices and Testing Machines (Basic Principles)*, Physikalisch-Technische Bundesanstalt (PTB), Braunschweig, Germany, 2017.

LIYUE FU (Student Member, IEEE) received the M.S. degree in biomedical engineering from Shandong University, Jinan, China, in 2009. She is currently pursuing the Ph.D. degree in instrument science and technology with Southeast University, China. She focuses her work on robot sensing and control technology.

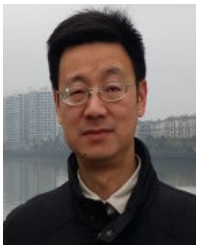

AIGUO SONG (Senior Member, IEEE) received the B.S. degree in automatic control and the M.S. degree in measurement and control from the Nanjing University of Aeronautics and Astronautics, Nanjing, China, in 1990 and 1993, respectively, and the Ph.D. degree in measurement and control from Southeast University, Nanjing, in 1996. From 1996 to 1998, he was an Associate Researcher with the Intelligent Information Processing Laboratory, Southeast University. From 1998 to 2000, he was an Associate Professor with the Department of Instrument Science and Engineering, Southeast University. From 2000 to 2003, he was the Director of the Robot Sensor and Control Lab, Southeast University. From April 2003 to April 2004, he was a Visiting Scientist with the Laboratory for Intelligent Mechanical Systems, Northwestern University, Evanston, IL, USA. He is currently a Professor with the School of Instrument Science and Engineering, Southeast University. His research interests include haptic display, robot tactile sensor, and telerehabilitation robot. He is a member of the Chinese Instrument and Control Association.